

# On bond failure by splitting of concrete cover surrounding anchored bars

M. Talaat & K.M. Mosalam

*Department of Civil and Environmental Engineering, University of California, Berkeley, USA*

**ABSTRACT:** This study develops analytical expressions for the bond stress level surrounding a longitudinal steel bar that causes the cover concrete to fail in a splitting mode, with bar-to-surface cracks forming in the longitudinal direction parallel to the bar. The proposed models use as a foundation the fracture mechanics-based cohesive-elastic ring model, developed by Reinhardt & Van der Veen (1990) based on original work by Tepfers (1979). They propose formulations that better address the assumptions and simplifications made in the original model, namely the biaxial behavior of concrete in tension, the crack-opening displacement profile, and the material law governing post-cracking tension softening. The relative significance of the proposed model enhancements is established through their prediction of bond stress and the associated computational cost for a computational benchmark problem involving a steel bar pullout from a concrete cylinder. Finally, the robustness of the reference and proposed models, measured by their sensitivity to the uncertainty in their respective parameters is evaluated and compared using a deterministic sensitivity analysis. Based on such analysis, recommendations are given on the most suitable and practical enhancements of the original model.

## 1 INTRODUCTION

### 1.1 Motivation

The use of Fracture Mechanics (FM) in estimating concrete behavior and determining the strength of concrete elements has received considerable attention over the past years, primarily because it can describe and interpret size effects in the experimentally-observed behavior of concrete structures. In the field of applying FM to concrete, two approaches came to be widely accepted within the engineering community, both of which adopt the assumptions of Linear Elastic Fracture Mechanics (LEFM). The first is the Fictitious Crack Model (FCM) due to Hillerborg et al (1976). The second approach is the Crack Band Theory model, introduced by Bazant and Oh (1983). Of the two, the former has an advantage of not relying on an empirical parameter such as the crack band width, which makes it more readily adaptable for implementation in Finite Element (FE) codes. The FCM approach has been used to develop the cohesive-elastic bond-splitting model for estimating the cover-splitting strength along a reinforcing steel bar based on bond stress (Tepfers 1979). In this study, this original model is designated  $A_0$  and is briefly reviewed for completeness and its simplifying assumptions identified. Four alternative models are developed and introduced to mathematically address these assumptions and des-

ignated  $A_1$  through  $A_4$ . The proposed models are compared through their estimation of bond strength in a typical bar pull-out example of a steel bar embedded in a concrete cylinder. After identifying the more significant models among the proposed alternatives, the stability of their predictions with respect to the uncertainty in their individual parameter values is investigated using a deterministic sensitivity analysis, namely the Tornado diagram analysis (Lee & Mosalam 2005) and compared to that of the reference model within the context of the benchmark problem. Besides establishing the sensitivity to modeling assumptions, the discussion of the benchmark problem results addresses the influence and methods of selection for the number of radial cracks in the model under both deterministic and probabilistic contexts.

### 1.2 Background – Model $A_0$

The reference bond-splitting model assumes the distribution of stresses and deformations shown in Figure 1 for a single bar embedded in concrete. As the bar is being pulled from the concrete, ribs on its perimeter result in an inclined resisting force, which can be resolved into radial “pressure” and longitudinal “bond” components, related through an angle of internal friction  $\alpha$ , which reflects the surface conditions. The stress state is assumed axi-symmetric at

any radius  $r$ . The cylinder enclosed within the cover  $c$  surrounding the bar is assumed to have  $n$  identical and stable cracks that extend radially to a length  $e$ . A polar coordinate system is used where the radial and tangential directions are indicated by subscripts  $r$  and  $t$ , respectively. The hoop (tangential) stress at  $r = e$  is equal to the cracking stress  $f_t$ , and is assumed to vary elastically in the uncracked region,  $r > e$ . The model assumes that neighboring longitudinal bars are far enough and that their bond stress fields do not overlap. In the cracked region,  $r \leq e$ , the tangential stress decreases towards the center with the widening of the crack width  $w$  until it vanishes at a crack width  $w_c$ , following a power law as follows,

$$\sigma_t(w)/f_t = 1 - (w/w_c)^{k_0} \quad (1)$$

where  $k_0$  = material parameter determined from the tensile fracture energy  $G_F$ . The hoop strain at  $r = e$ , neglecting Poisson's effect, is obtained from

$$\varepsilon_r(e) = f_t/E_c \equiv \varepsilon_{cr} \quad (2)$$

where  $E_c$  = concrete modulus of elasticity. This value of the radial strain is assumed constant over the cracked part  $r \leq e$ . Thus,

$$2\pi\varepsilon_r(e) = 2\pi\varepsilon_r(r) + nw(r), \quad \varepsilon_r(r) \approx \varepsilon_r(e) = \varepsilon_{cr} \quad (3a, b)$$

This yields a linear distribution of crack width, i.e.

$$w(r) = 2\pi\varepsilon_{cr}(e-r)/n \quad \text{for } r \leq e \quad (4)$$

which gives an explicit formula for the hoop stress in the cracked region, namely,

$$\sigma_t(r) = \sigma(w(r)) \quad \text{for } r_m \leq r \leq e \quad (5)$$

where  $r_m = \max \{d_s/2, e - w_c/2\pi\varepsilon_{cr}\}$  defines the end of the cohesive zone where softening occurs.

Given the elastic solution (Timoshenko & Goodier 1951) of stresses at radius  $r$ , in a thick-walled cylinder of  $r_i$  and  $r_o$  inner and outer radii, respectively, subjected to internal pressure  $p_i$ , i.e.

$$\begin{aligned} \sigma_r(r) &= p_i \frac{r_i^2}{r_o^2 - r_i^2} \left( 1 - \frac{r_o^2}{r^2} \right) \\ \sigma_t(r) &= p_i \frac{r_i^2}{r_o^2 - r_i^2} \left( 1 + \frac{r_o^2}{r^2} \right) \end{aligned} \quad \text{for } r \geq e \quad (6a, b)$$

The pressure  $p$  at the bar surface contributed by both regions, elastic and cracked, can then be calculated by superposition of the equilibrium solution for the elastic region and the integral of  $\sigma_t(r)$  over  $r \leq e$ .

### 1.2.1 Elastic Contribution, $p_e$

From Equation 6b we can deduce the pressure acting at the bar surface given the pressure applied at the inner wall of the elastic ring. Hence,

$$p_e = \frac{e}{d_s/2} p_i = \frac{2e}{d_s} f_t \frac{(c+d_s/2)^2 - e^2}{(c+d_s/2)^2 + e^2} \quad (7)$$

where  $\sigma_t(e) = f_t$  at the onset of cracking,  $d_s$  = bar diameter  $r = r_i = e$ , and  $r_o = c + d_s/2$  in Equation 6.

### 1.2.2 Cohesive Contribution, $p_c$

At any radius  $r \leq e$ , for the rigid body mechanism assuming Equation 3 holds, using Equations 1, 4, and 5 and finally integrating the hoop stresses over the cracked region leads to

$$\begin{aligned} p_c &= \frac{f_t}{d_s/2} \int_e^{r_m} \frac{\sigma_t(w(r))}{f_t} dr = \frac{2f_t}{d_s} \int_e^{r_m} \left[ 1 - \left( \frac{w(r)}{w_c} \right)^{k_0} \right] dr \\ &= \frac{2f_t}{d_s} (e - r_m) \left\{ 1 - \frac{1}{k_0 + 1} \left[ \frac{2\pi\varepsilon_{cr}}{nw_c} (e - r_m) \right]^{k_0} \right\} \end{aligned} \quad (8)$$

Superposing Equations 7 and 8 leads to the total pressure, namely

$$p = p_e + p_c \quad (9)$$

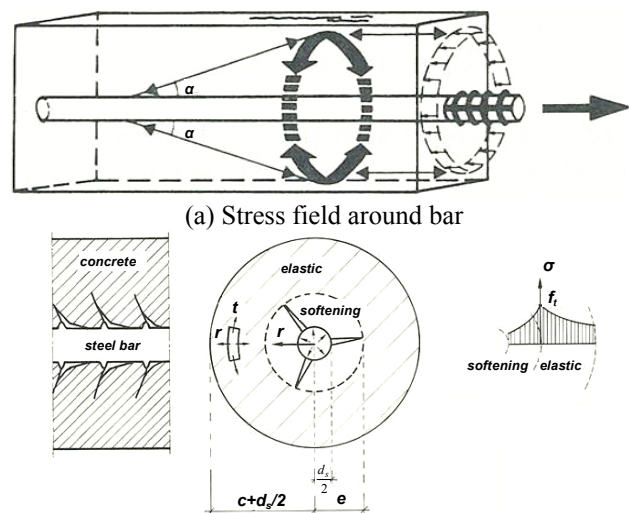
Subsequently, from equilibrium, the shear stress is

$$\tau = p \tan \alpha \quad (10)$$

which represents the bond strength at crack length  $e$ . Eligehausen et al. (1983) calculated the average value of the angle of internal friction  $\alpha$ , using numerical results of stress distribution around a bar with lateral ribs for a range of cover thickness and bar diameter values. The results were independent of the concrete quality, with values varying between 0.49 and 1.00. Presently,  $\alpha$  is left out by restricting the computation to the radial pressure  $p$  due to the ribs on the bar and the pull-out action of the longitudinal stress. Thus, the pressure capacity is given by

$$p_r = \max_e \{p\} \quad (11)$$

where  $p_r$  = the maximum pressure value the ring can sustain as the crack propagates radially, after which the crack becomes unstable and runs all the way to the surface causing a longitudinal splitting crack.



(b) Cohesive-elastic ring idealization of cover region  
Figure 1. Cohesive-elastic crack model (Tepfers 1979, Reinhardt & Van der Veen 1990).

This value is dependent on the assumed number of radial cracks  $n$  whose increase results in a decrease in the crack opening  $w$  per crack at any given crack length  $e$ , which leads to an increase in the average tangential stress within the cracked region and a corresponding increase in the cohesive pressure term  $p_c$ . The secondary effect of discretely-spaced transverse reinforcement is not explicitly modeled in this model yet can be included in the parameter  $\alpha$ .

## 2 MODEL ENHANCEMENTS

A close investigation of Equation 9 reveals that the resulting pressure is directly proportional to the tensile strength  $f_t$ , fracture energy  $G_F$ , cover thickness  $c$ , number of cracks  $n$ , and limiting crack width  $w_c$ , while it is inversely proportional to the reinforcing bar diameter  $d_s$ . However, this model involves the following assumptions and simplifications:

- 1 The concrete material is assumed to behave uniaxially. This is reflected in neglecting the effect of radial dilation in calculating  $\varepsilon_{cr}$  in Equation 2, as well as assuming that cracking in tension takes place upon violating a uniaxial stress criterion in the hoop direction which neglects the effect of the radial stress. This radial stress is compressive for the given deformation mode, which should reduce the uniaxial tensile strength and lead to unconservative estimates using model  $A_0$ .
- 2 The crack opening is assumed to vary linearly with the radius in Equation 4. This requires that the tangential strain along the crack length is equal to the cracking strain, which is only valid at  $r = e$  (Equation 3). Softening in the region  $r < e$  will result in the bulk material between cracks elastically unloading to lower strains and, subsequently, a non-linear crack width distribution along the radius  $r$ . This is neglected, with the argument being made that a compensating effect is expected from neglecting radial dilation.
- 3 The model assumes that the exact shape of the tension softening relationship does not significantly affect the resulting strength, as long as the fracture energy enclosed by the softening curve remains the same. Thus, the model adopts a simple power softening law (Equation 1), whose coefficient  $k_0$  is determined by equating to  $G_F$  the integral of  $\sigma dw$  over the range  $0 < w < w_c$ . Furthermore, while  $f_t$  is either directly measured or estimated from the compressive strength,  $G_F$  is difficult to measure and is commonly estimated as a function of  $f_t$ , and  $w_c$  is typically estimated as a multiple of the average aggregate size (Ratanalert & Wecharatana 1989), leading to compounded uncertainty in the model estimation.

The following subsections will present the mathematical formulations developed to address each of the individual assumptions identified above.

### 2.1 Model $A_1$ – Biaxial behavior of concrete

The introduction of a concrete biaxial failure criterion explicitly accounts for the effect of radial dilation in the cracked region. The modified cracking stress  $f_t'$  is adopted from Gambarova et al. (1994),

$$f_t' = f_t \left( 1 + 0.8 \frac{\sigma_r(e)}{f_c} \right) \quad (12)$$

where  $f_c$  = compressive strength and  $\sigma_r$  = radial (transverse) stress (tension positive). Dividing Equation 6a by Equation 6b and setting  $\sigma_t(e) = f_t'$ ,

$$\sigma_r(e) = -f_t \left[ \frac{(c + d_s/2)^2 + e^2}{(c + d_s/2)^2 - e^2} + \frac{0.8f_t}{f_c} \right]^{-1} \quad (13)$$

Substituting Equation 13 in Equation 6 and solving for  $p_e$  as in Equation 7 leads to the first term in Equation 14. The second term is analogous to that in Equation 9 after replacing  $f_t$  by  $f_t'$ . Accordingly, the total pressure sustained in the ring surrounding the bar is given by

$$p = \frac{2f_t}{d_s} (e) \left[ \frac{(c + d_s/2)^2 + e^2}{(c + d_s/2)^2 - e^2} + \frac{0.8f_t}{f_c} \right]^{-1} + \frac{2f_t'}{d_s} (e - r_m) \left\{ 1 - \frac{1}{k_0 + 1} \left[ \frac{w_m}{w_c} \right]^{k_0} \right\} \quad (14)$$

where the crack width  $w_m$  = the smaller of  $w_c$  and the crack width at the steel-concrete interface, and can be expressed as

$$w_m = (2\pi\varepsilon_{cr}(e - r_m))/n \quad (15)$$

Equation 14 explicitly incorporates the effect of the biaxial stress state in the plane of the bar cross-section on the tensile cracking in concrete. The model becomes further complicated upon considering 3-D stress state effects. However, it is argued that splitting failure is investigated in between two existing flexural cracks and that concrete stresses in the longitudinal direction are therefore insignificant. It is also assumed that stress fields surrounding neighboring longitudinal bars are far enough relative to the cover thickness. The effect of radial dilation is accounted for by updating  $\varepsilon_{cr}$  in Equation 16 for each trial crack length  $e$  according to

$$\varepsilon_{cr}(e) = (f_t - \nu\sigma_r(e))/E_c \quad (16)$$

where  $\nu$  = Poisson's ratio for concrete.

### 2.2 Model $A_2$ – Nonlinear crack width distribution

Accounting for the nonlinear crack width distribution requires the solution of an iterative nonlinear problem. The governing compatibility equation is

$$2\pi r \varepsilon_t(r) + n w(r) = 2\pi r \varepsilon_t(e) \approx 2\pi e \varepsilon_{cr} \quad (17)$$

Thus, along the crack face, according to Equation 1 the tangential stress distribution follows Equation 18; while in the bulk concrete between two cracks, assuming uniform linear-elastic unloading, the tangential stress distribution follows Equation 19. Finally, invoking equilibrium requires equality between Equations 18 and 19.

$$\sigma_t(r) = f_t \left( 1 - (w(r)/w_c)^{k_0} \right) \quad (18)$$

$$\sigma_t(r) = E_c \varepsilon_t(r) \quad (19)$$

Substituting Equation 19 in Equation 17 leads to

$$nw(r) = 2\pi(e\varepsilon_{cr} - r\sigma_t(r)/E_c) \quad (20)$$

Substituting Equation 20 in Equation 18 yields

$$\sigma_t(r) = f_t \left\{ 1 - \left( \frac{2\pi}{nw_c} [e\varepsilon_{cr} - r\sigma_t(r)/E_c] \right)^{k_0} \right\} \quad (21)$$

Equation 21 is nonlinear of the form  $x = G(x)$  for  $x = \sigma_t$ . Convergence requires that  $|dG(x)/dx| < 1$ . This is indeed satisfied, as illustrated by Equation 22

$$\frac{dG(\sigma_t(r))}{d\sigma_t(r)} = \left( \frac{2\pi}{nw_c} \right)^{k_0} \frac{k_0 r f_t}{E_c} [e\varepsilon_{cr} - r\sigma_t(r)/E_c]^{(k_0-1)} \quad (22)$$

Numerical investigation of typical parameter ranges suggest that the solution will converge, albeit slowly. After evaluating the hoop stress at sufficient points along the radius, the pressure in the ring is calculated by numerical integration of Equation 8.

### 2.3 Models $A_3$ and $A_4$ – Alternate softening laws

Several tensile stress–crack width softening laws have been proposed in the literature. A recent review is available in van Mier (1997). An all-inclusive survey would be prohibitive and beyond the scope of this study. Instead, two alternative laws are considered and shown to have a significant effect on the results. Model  $A_3$  uses the tensile softening law given in Gambarova et al. (1994) by the formula

$$\sigma(w) = f_t \frac{1 - w/w_c}{1 + k_3 w/d_a} \quad (23)$$

where  $d_a$  = average aggregate size and  $k_3$  = model parameter. The elastic contribution to the total pressure  $p_e$  in Equation 9 is not affected by Equation 23. However, using Equation 23 for calculating the derivative  $dr/dw$  and noting that  $w$  decreases as  $r$  increases, the cohesive contribution  $p_c$  becomes

$$p_c = \frac{f_t}{d_s/2} \int_e^{r_m} \frac{\sigma_t(w(r))}{f_t} dr = \frac{2f_t}{d_s} \int_e^{r_m} \left[ \frac{1 - w(r)/w_c}{1 + k_3 w(r)/d_a} \right] dr \quad (24)$$

$$= \frac{nd_a f_t}{\pi k_3 w_c \varepsilon_{cr} d_s} \left\{ -w_m + \left( 1 + \frac{k_3 w_c}{d_a} \right) \left( \frac{d_a}{k_3} \right) \ln \left[ 1 + \frac{k_3 w_m}{d_a} \right] \right\}$$

Model  $A_4$  uses an alternate form of the power law in Equation 1, according to

$$\sigma_t(w)/f_t = (1 - w/w_c)^{k_4} \quad (25)$$

where  $k_4$  = model parameter. This leads to the cohesive pressure term in Equation 9 becoming

$$p_c = \frac{2f_t}{d_s} \int_e^{r_m} \left( 1 - \frac{w(r)}{w_c} \right)^{k_4} dr = \frac{nw_c f_t}{\pi(k_4 + 1) \varepsilon_{cr} d_s} \left[ 1 - \frac{2\pi \varepsilon_{cr}}{nw_c} (e - r_m) \right]^{(k_4+1)} \quad (26)$$

For the purpose of comparing models  $A_0$ ,  $A_3$  and  $A_4$  and isolating the shape effect of the tensile softening curve, parameters  $k_3$  and  $k_4$  are selected so that the tensile fracture energy  $G_F$  under the softening curve in Equations 23 and 25 is maintained equal to that under the softening curve in Equation 1 for a corresponding value of  $k_0$ . Figure 2 presents graphic comparison of the alternate softening laws.

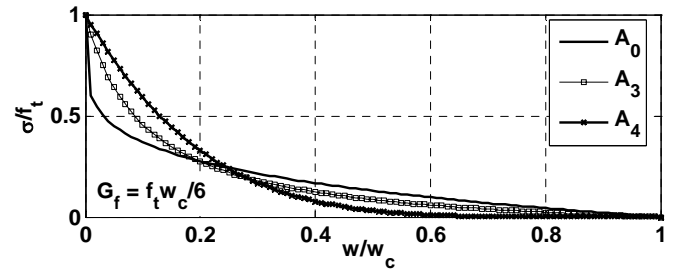


Figure 2. Tension-softening profiles for equal fracture energy.

## 3 BENCHMARK PROBLEM

The relative significance of the enhancements described in Section 2 is evaluated using a hypothetical benchmark problem of typical parameter values. This benchmark problem considers the bar-pullout resistance of a single reinforcing steel bar embedded in a concrete cylinder and evaluates the maximum radial pressure developed before bond-splitting failure occurs. The radial pressure is computed and maximized along the crack length for a variable number of radial cracks. The estimated response using model  $A_0$  is compared to estimates using models  $A_1$  through  $A_4$  to investigate the sensitivity to the individual simplifying assumptions. The computational time needed by each model is also compared to assess its practicality. In addition, the sensitivity of the model estimate to the assumed number of cracks is investigated and combined with experimental observations to estimate a value for the parameter  $n$  in the absence of experimental data pertinent to the problem of interest. In the presence of such data, a probabilistic approach is outlined to account for randomness in  $n$ .

### 3.1 Problem statement

The benchmark problem geometry is similar to Figure 1. Since the governing equations are highly nonlinear, the use of normalized quantities for force

and geometric parameters becomes a matter of form and convenience, because the results remain specific to the neighborhood of the set of geometric and material properties considered. As such, the significance of the different model enhancements, discussed above, is investigated on a problem that represents a commonly encountered set of parameters. The problem data is as given below:

$f_c = 30.0$  MPa,  $w_c = 0.2$  mm,  $f_t = 3.0$  MPa,  $c = 30.0$  mm,  $E_c = 22.0$  GPa,  $d_s = 10.0$  mm,  $G_F = 0.1$  MPa.mm,  $d_a = 16.0$  mm, and  $\nu = 0.2$ . This data yield the model parameters  $k_0 = 0.2$  in Equation 1,  $k_3 = 773.0$  in Equation 23, and  $k_4 = 5.0$  in Equation 25.

### 3.2 Comparison Results

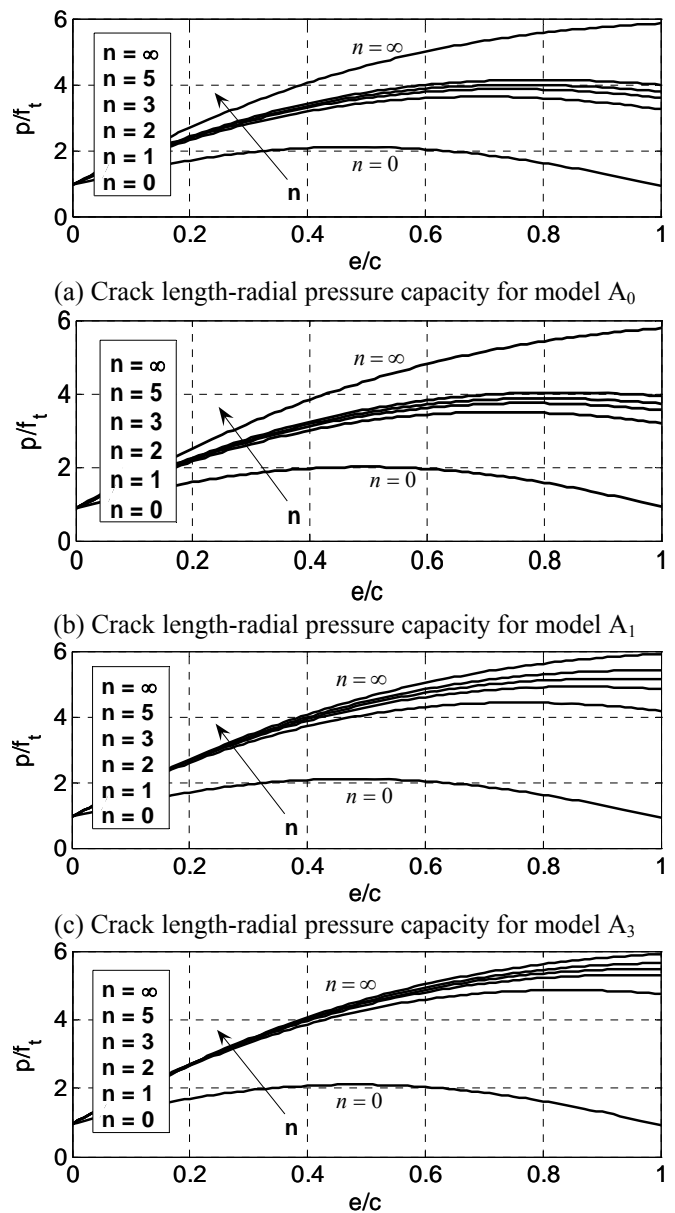
Figure 3 shows the computational solutions calculated for the benchmark problem using models  $A_0$ ,  $A_1$ ,  $A_3$  and  $A_4$ . Results for model  $A_2$  are not noticeably different from those of model  $A_0$  and are not shown. The plots demonstrate the variation of the normalized radial pressure capacity  $p/f_t$ , versus the normalized radial crack length  $e/c$ , for a range of assumed radial cracks  $n$ . The number of cracks range from 0 to  $\infty$ . The case  $n = 0$  corresponds to an assumption of  $p_c = 0$  and no cohesion in the cracked concrete, i.e. brittle tensile cracking. The case  $n = \infty$  corresponds to a case of an infinitely-rigid confining medium outside the cover region. Together, both cases define the theoretical bounds on the solution.

It can be observed that the radial pressure capacity is positively correlated to the number of radial cracks, and that it increases as a result of increasing crack length up to a maximum value and then decreases as the crack becomes unstable and splitting failure occurs. It can also be observed that the normalized radial pressure values computed using model  $A_0$  are generally higher than those of model  $A_1$  and lower than those of model  $A_2$ .

Given Equation 11, the radial pressure capacity pertinent to the bond-splitting failure is the maximum response in Figure 3 at each  $n$  value and can be determined numerically. These values have been computed for  $n = 1, 2, \text{ and } 3$  for models  $A_0$  through  $A_4$  and tabulated in Table 1. The computational time required for completing the solution is also indicated for each model. For ease of comparison, all values in the table have been normalized by the corresponding value (on the same row) for Model  $A_0$ .

Table 1. Comparison between radial pressure capacity of reference and alternative models.

$n$	Model $A_0$	Model $A_1$	Model $A_2$	Model $A_3$	Model $A_4$
1	1.000	0.969	1.060	1.220	1.339
2	1.000	0.972	1.053	1.273	1.372
3	1.000	0.973	1.049	1.293	1.376
Time	1.000	1.333	192.300	0.667	1.000



(a) Crack length-radial pressure capacity for model  $A_0$   
(b) Crack length-radial pressure capacity for model  $A_1$   
(c) Crack length-radial pressure capacity for model  $A_3$   
(d) Crack length-radial pressure capacity for model  $A_4$   
Figure 3. Partial results for benchmark problem.

### 3.3 Discussion

This section discusses the behavior of the computed response using model  $A_0$  and its dependency on the assumed number of radial cracks, and compares its predictions with those of models  $A_1$  through  $A_4$  to establish the effect of their underlying assumptions. In discussing the model sensitivity to the number of radial cracks in section 3.3.1, the comparison is limited to models  $A_0$ ,  $A_3$ , and  $A_4$ . This is because the predicted response of models  $A_1$  and  $A_2$  is not significantly different from that of model  $A_0$ .

#### 3.3.1 Effect of number of radial cracks

It is clear in Figure 3 that the influence of  $n$  affects primarily the peak pressure capacity, while its effect on the computed response at lower  $e/c$  values is less significant. The computed response experiences a major increase upon considering the cohesion contribution (from  $n = 0$  to 1), and that the sensitivity decreases quickly as  $n$  increases further. A conserva-

tive estimate of  $n = 1$  is typically assumed in design situations for choosing appropriate cover thickness and bar anchorage lengths. However, experimental observations by Reinhardt et al. (1986) report a consistent observation of three cracks or more. It can also be argued that the assumption of an axisymmetric stress state, upon which the model formulation is based, is grossly violated by the assumption of one radial crack.

Figure 3 shows that the sensitivity of the model prediction to the uncertainty in the number of radial cracks for values of  $n > 1$  is highest in the reference model  $A_0$ . This sensitivity decreases significantly in model  $A_3$  and is minimal for model  $A_4$  (11% increase in  $p_r$  from  $n = 2$  to  $n = \infty$ , versus 20% and 51% increases for  $A_3$  and  $A_0$ , respectively). In the range of commonly-observed values of  $n$  between 2 and 5, the sensitivity in prediction for the three models is comparable and is equal to 7%, 11% and 6% for  $A_0$ ,  $A_3$ , and  $A_4$ , respectively.

It must be noted that the number of radial cracks is a function of the geometry and boundary conditions surrounding the embedded longitudinal bar, which may differ from the idealized benchmark problem. Therefore, one concludes that an assumption of  $n = 2$  or 3 satisfies the model assumptions, results in a stable estimate, and conservatively agrees with experimental observations in cases where experimental data pertinent to the application of interest is not available. In the presence of application-specific experimental data, a probabilistic approach can be followed that mimics the randomness of the process; whereby  $n$  can be assigned a discrete probability distribution (e.g. Poisson) whose parameters can be estimated from the data. By simulating  $n$  a sufficient number of times from this assigned distribution and substituting in the bond-splitting model, the distribution of the resulting bond strength can be generated and its mean and dispersion estimated.

### 3.3.2 Effect of biaxial behavior of concrete

It can be observed in Table 1 and Figure 3b that incorporating the biaxial behavior of concrete has no significant effects on the estimated response. The observed effect results in a decrease of the estimated maximum radial pressure capacity and an increase of the  $e/c$  value where the maximum capacity is obtained. On average, radial pressure capacity values computed using model  $A_1$  for the benchmark problem are consistently less than those computed using model  $A_0$  by approximately 3%. This results in unconservative estimates but is compensated for by the assumption of linear crack width distribution.

### 3.3.3 Effect of nonlinear crack width distribution

It can be observed in Table 1 that accounting for nonlinear crack width distribution in model  $A_2$  results in an increase in the estimated radial pressure

capacity by approximately 5% and requires approximately 200 times more CPU time for the benchmark problem. The increase in accuracy is deemed infeasible and unjustified for modeling such a local phenomenon in the context of an FE model, especially because the increased accuracy does not render the original model unconservative. Thus, the initial simplifying assumption of neglecting this effect is considered adequate and justified.

### 3.3.4 Effect of softening law

It can be observed in Table 1 and Figure 3c and d that, counter to commonly assumed, the shape of the softening curve does result in a significant effect both on the radial pressure capacity and the corresponding  $e/c$  value. For model  $A_3$ , the difference in estimated maximum pressure capacities is approximately 28%, while for model  $A_4$ , the difference is approximately 37%; for  $n$  ranging between 2 and 5 cracks. This is evidence that the designation of the fracture energy as a sole parameter – in addition to its being usually empirically assumed rather than directly measured and thus highly uncertain – instead of a more accurate representation of the actual post-cracking behavior is a major source of uncertainty for this model.

## 4 DETERMINISTIC SENSITIVITY ANALYSIS

It has been established in the previous section that the assumption of alternative material softening laws and the use of cohesive-elastic bond splitting models formulated accordingly leads to a significant variation in the predicted response across these models, namely  $A_1$ ,  $A_3$ , and  $A_4$ . Therefore, the adoption of tensile fracture energy as a sole model parameter to characterize the softening behavior is a major source of uncertainty in the model. This uncertainty is further compounded by the uncertainty in the tensile fracture energy value, which is often estimated from indirect measurements. This section individually examines the robustness of the three models  $A_0$ ,  $A_3$ , and  $A_4$  by investigating the sensitivity of the response predicted within each model to the model input parameters. The comparative study is performed using a deterministic sensitivity analysis approach, commonly referred to in the literature as the Tornado diagram analysis method. A summary of this method is described next. An extensive review can be found in (Lee & Mosalam 2005) and a similar application of this approach to the present study can be found in (Binici & Mosalam 2007).

The Tornado diagram analysis is a deterministic method developed to numerically determine the sensitivity of an output quantity of interest to uncertainty in input parameter values, and thus establish the relative importance of the input parameters with respect to their random nature. In this method, a ref-

reference point is initially set by computing the predicted model response using the expected mean values of the input parameters. Next, the parameters are individually varied within a given range of uncertainty, typically parameterized by their coefficient of variation (COV). The resulting changes (swings) in the predicted response quantity is computed, compared and sorted across the different parameters. A graphic comparison of the computed sensitivity measures (swings) is used to establish the relative importance of the parameters. A larger sensitivity measure is an indication of a higher relative importance of the associated parameter and, consequently, a larger role for the uncertainty associated with said parameter in determining the outcome and accuracy of the model. In interpreting the results for the comparative study, the following criteria are considered to indicate a higher degree of model robustness: (a) Relatively lower sensitivity to uncertainty in input parameters, (b) significant sensitivity to only a smaller number of parameters, and (c) especially low sensitivity to parameters in which a higher degree of uncertainty is anticipated.

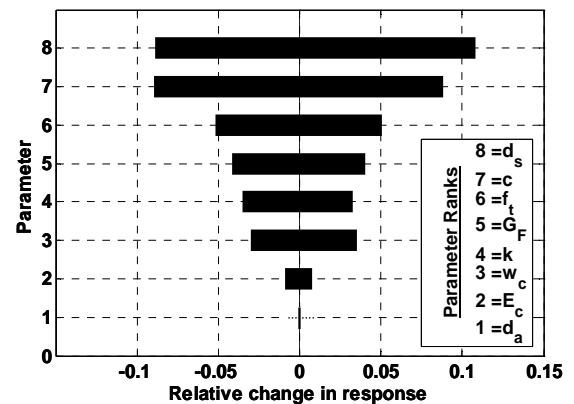
#### 4.1 Problem statement

The benchmark problem defined in section 3 is used in the present Tornado diagram analysis. The predicted maximum pressure  $p_r$  is defined as the output quantity of interest. The list of input parameters being considered and their mean values is composed of the quantities defined at the end of subsection 3.1. The deterministic sensitivity of the model response to parameter uncertainty is calculated using the relative change (swing) in the predicted maximum pressure corresponding to one standard deviation step on either side of the mean value for each input parameter, with an assumed COV of 10%. Since the model sensitivity to parameter uncertainty is generally nonlinear, a tight step size (in terms of COV) is recommended in order to better represent the sensitivity in the neighborhood of the mean response.

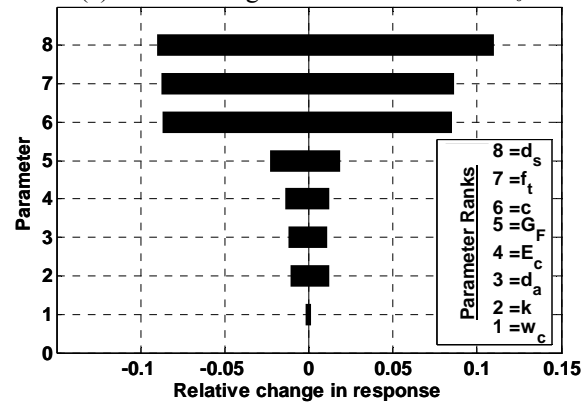
#### 4.2 Results

Figure 4 shows the Tornado diagram results for models  $A_0$ ,  $A_3$ , and  $A_4$ , where the parameter  $k$  represents softening law parameters  $k_0$ ,  $k_3$ , and  $k_4$ , respectively. The shown results correspond to the case of  $n = 3$ . The most important model parameter is the bar diameter, and it has the same sensitivity measure for all models. This is followed by the cover thickness then tensile strength (order reversed for  $A_1$ ) at approximately equal importance. The fourth parameter on the list is tensile fracture energy, where there is a significant difference in the sensitivity measure across models. Here starts a significant decrease in importance for the remaining parameter in models  $A_3$  and  $A_4$ , but not in model  $A_0$ . The relative impor-

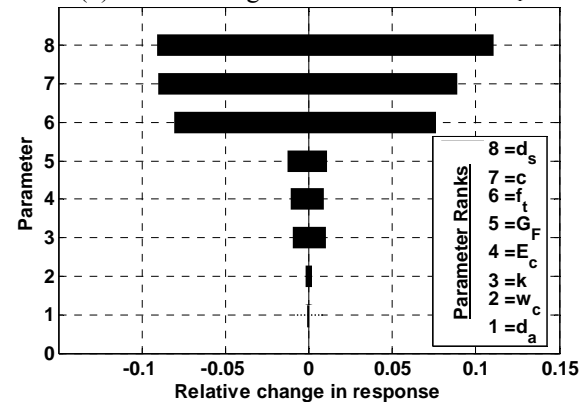
tance of the subsequent variables continues to decrease. The minimum sensitivity measure value is zero for the average aggregate size in models  $A_0$  and  $A_4$ , where it is not included in the softening law formulation. Regarding uncertainty in the power law parameters  $k$ , model  $A_0$  is most sensitive with parameter  $k_0$  having an importance rank of 4 out of 8. Parameter  $k_3$  has a rank of 2 in model  $A_3$ , while  $k_4$  has a rank of 3 in model  $A_4$ . However the value of the sensitivity measure indicates that model  $A_3$  is slightly more sensitive to parameter  $k_3$  than model  $A_4$  is to parameter  $k_4$ . It is worth noting that the sensitivity of models towards the assumed 10% COV is commensurable with their sensitivity to the number of radial cracks over their range of expected values (subsection 3.3.1). Thus, for parameters whose expected COV is typically lower (e.g. bar diameter), or typically higher (e.g. fracture energy), the relative importance of the number of cracks can be deduced.



(a) Tornado diagram results for model  $A_0$



(b) Tornado diagram results for model  $A_1$



(c) Tornado diagram results for model  $A_3$

Figure 4. Results of Tornado diagram for  $n = 3$  radial cracks.

### 4.3 Discussion

Referring to the criteria of model robustness outlined earlier in section 4, all models display approximately the same sensitivity towards the three highest-ranking parameters. These three parameters are typically easier to estimate or measure directly with limited uncertainty. However, models  $A_3$  and  $A_4$  do not display significant sensitivity towards the remaining parameters, whereas model  $A_0$  does. Moreover, model  $A_0$  is significantly sensitive to the fracture energy, whose estimation typically involves high uncertainty, and to the power law parameters  $k_0$  and  $w_c$ , which are highly uncertain owing to perceived randomness in tension-softening response. Therefore, the proposed models  $A_3$  and  $A_4$  are more robust than the reference model  $A_0$ . This is further reinforced by the relative sensitivity of the three models to the number of radial cracks previously observed in subsection 3.3.1. Moreover, since model  $A_4$  displays less sensitivity towards uncertainty in the remaining parameters than model  $A_3$ , is not affected by the uncertainty in estimating the average aggregate size, and shows decreasing sensitivity towards fracture energy and the lower-ranking parameters with increased number of radial cracks (not shown), it is considered the most robust model.

## 5 CONCLUDING REMARKS

From the previous discussions, the following concluding remarks can be inferred:

1. The cohesive-elastic model for bond failure between concrete and longitudinal steel bars by splitting has been reviewed, and its assumptions and simplifications have been identified for investigation. Four alternate models have been formulated to explicitly address each assumption.
2. A benchmark problem has been introduced to assess the relative significance of improving the individual modeling assumptions.
3. It has been demonstrated that ignoring the biaxial behavior of concrete in tension results in an insignificant overestimation of bond strength. This effect is counter-balanced by the equally insignificant effect of assuming linear crack width distribution along the crack length.
4. It has been demonstrated that the shape of the tension-softening material law is a significant factor of uncertainty in the analytical model, and that it is important to select a softening law that reliably represents the considered application.
5. The model sensitivity to the number of radial cracks has been investigated. Recommendations for selecting a valid estimate in both deterministic and probabilistic contexts were presented.
6. The relative robustness against parameter uncertainty in the reference model as well as two mod-

els formulated using alternative tension-softening material laws was assessed using a Tornado diagram analysis for the benchmark problem.

7. The reference model was found to be relatively most sensitive to uncertainty in parameters which typically have a highly random nature and thus is the least robust. The two alternate models were found to be significantly less sensitive to highly-random parameters and should therefore result in a more reliable prediction of bond strength.

## ACKNOWLEDGMENT

This study is supported by the Earthquake Engineering Research Centers Program of the NSF under Award No. EEC-9701568 to PEER at UC Berkeley. Opinions and findings presented are those of the authors and do not reflect views of the sponsors.

## REFERENCES

- Bazant, Z & Oh, B. 1983. Crack band theory for fracture of concrete. *Materials and Structures*. 16(93): 155-177.
- Binici, B. & Mosalam, K. 2007. Analysis of reinforced concrete columns retrofitted with fiber reinforced polymer lamina. *Composites B: Engineering*. 38(2): 265-276.
- Eligehausen, R., Popov, E. & Bertero, V. 1983. Local bond stress-slip relationships of deformed bars under generalized excitations. *UCB/EERC-83/23*. Earthquake Eng. Research Center, Univ. of California, Berkeley, USA.
- Gambarova, P., Rosati, G & Schumm, C. 1994. An elasto-cohesive model for steel-concrete bond. In Bazant, Bitnar, Jirasek, & Mazars (eds) *Fracture and Damage in Quasibrittle Structures: Experiment, Modeling, and Computer Analysis*. Chapman and Hall: 557-566.
- Hillerborg, A, Modeer, M. & Petersson, P. 1976. Analysis of crack formation and crack growth in concrete by means of fracture mechanics and finite elements. *Cement and Concrete Research*. 6: 773-782.
- Lee, T.-H. & Mosalam, K. 2005. Seismic demand sensitivity of reinforced concrete shear-wall building using FOSM method. *Earthquake Engineering and Structural Dynamics*. 34(14): 1719-1736.
- Ratanalert, S, & Wecharatana, M. 1989. Evaluation of existing fracture models in concrete. In Li & Bazant (eds) *Fracture Mechanics: Application to Concrete*. ACI SP-118: 113-146.
- Reinhardt, H & Van der Vein, C. 1990. Splitting failure of a strain-softening material due to bond stresses. In Carpentieri (ed.), *Application of Fracture Mechanics to Reinforced Concrete*. Elsevier Applied Science: 333-346.
- Reinhardt, H, Corneilssen, H. & Hordijk, D. 1986. Tensile tests and failure analysis of concrete. *Journal of Structural Engineering*. ASCE. 112(11): 2462-2477.
- Tepfers, R. 1979. Cracking of reinforced concrete cover along anchored deformed reinforcing bars. *Magazine of Concrete Research*. 31(106): 3-12.
- Timoshenko, S. & Goodier, J. (2<sup>nd</sup> Ed.) 1951. *Theory of Elasticity*. McGraw-Hill.
- Van Mier, J. 1997. *Fracture Processes of Concrete*. CRC Press.